RISK AND VULNERABILITY ANALYSIS OF SATELLITES DUE TO MM/SD WITH PIRAT

Scott Kempf[(1)], Frank Schäfer[(1)], Martin Rudolph[(1)], Nathan Welty[(1)], Thérèse Donath[(2)], Roberto Destefanis[(3)], Lilith Grassi[(3)], Rolf Janovsky[(4)], Leanne Evans[(4)], Arne Winterboer[(4)]

[(1)] Fraunhofer Institute for High-Speed Dynamics, Ernst-Mach-Institut, EMI, Eckerstr. 4, 79104 Freiburg, German, Email: scott.kempf@emi.fraunhofer.de
[(2)] ONERA-DCPS, Chemin de la Huniere, 91123 Palaiseau, France, Email: therese.donath@onera.fr
[(3)] Thales Alenia Space, Strada di Collegno, 253, 10146 Torino, Italy, Email: roberto.destefanis@thalesaleniaspace.com
[(4)] OHB System AG, Universitätsallee 27-29, 28359 Bremen, Germany, Email: Janovsky@ohb-system.de

ABSTRACT

Until recently, the state-of-the-art assessment of the threat posed to spacecraft by micrometeoroids and space debris was limited to the application of ballistic limit equations to the outer hull of a spacecraft. The probability of no penetration (PNP) is acceptable for assessing the risk and vulnerability of manned space mission, however, for unmanned missions, whereby penetrations of the spacecraft exterior do not necessarily constitute satellite or mission failure, these values are overly conservative.

The newly developed software tool PIRAT (Particle Impact Risk and Vulnerability Analysis Tool) has been developed based on the Schäfer-Ryan-Lambert (SRL) triple-wall ballistic limit equation (BLE), applicable for various satellite components. As a result, it has become possible to assess the individual failure rates of satellite components.

This paper demonstrates the modeling of an example satellite, the performance of a PIRAT analysis and the potential for subsequent design optimizations with respect of micrometeoroid and space debris (MM/SD) impact risk.

1 INTRODUCTION

The expansion of the space debris population and its threat to satellites is now a well-known and much discussed topic in space technology research. Especially in the LEO regime, the growth of space debris due to continued launches as well as the creation of new debris through cascading collisions poses a serious threat to satellites. The MEO and GEO regimes, although not as densely populated with space debris, remain dangerous, particularly due to higher velocity micrometeoroids.

In order to understand the dangers and effects of micrometeoroids and space debris (MM/SD), environmental debris models such as ESA's MASTER or NASA's ORDEM2000 have been developed. These provide debris flux information such as size, impact direction and debris velocity with respect to a spacecraft surface, with which information debris shielding and/or component redundancy can be applied and developed as a means of passive protection of the spacecraft. Ballistic limit equations (BLEs) have been developed to provide failure criteria for satellite external surfaces.

Existing risk analysis tools apply the above-mentioned debris models in order to estimate satellite structure penetration rates. The probability of no penetration (PNP) is particularly relevant to the analysis of manned-missions, such as the ISS. Penetration in the case of unmanned missions, however, does not automatically constitute failure of the satellite, nor does it automatically constitute the failure of any specific component. The Christiansen-Whipple and Cour-Palais BLEs, as well as the existing software tools, are not sufficient to provide accurate component-level failure rates for internal components [1]. For this reason, the Schäfer-Ryan-Lambert (SRL) BLE was developed during an earlier ESA study [2].

2 PIRAT METHODOLOGY

The Particle Impact Risk and Vulnerability Assessment Tool (PIRAT) was designed for the FP7 project P2-ROTECT for the purpose of calculating the statistically independent failure rates of internal components, which are shielded by structure panels. The software is based on the methodology developed in [1] and applies primarily the SRL BLE.

2.1 SRL ballistic limit equation

PIRAT uses the SRL triple-wall BLE for the analysis of the vulnerability of internal satellite components placed behind double panel structure walls to MM/SD. The applicability to internal satellite components for unmanned missions is due to the inclusion of the third wall, which represents the equipment cover plate located behind the satellite's outer structure and accounts for the inherent shielding capability of the internal components. The first two walls represent the

Proc. '6th European Conference on Space Debris'
Darmstadt, Germany, 22–25 April 2013 (ESA SP-723, August 2013)

satellite's outer structure, typically as aluminum honeycomb sandwich panels (H/C SP) or Whipple shields. Based on the Christiansen-Whipple BLE [3], the SRL BLE defines ballistic, shatter and hypervelocity regimes (3.0 and 7.0 km/s threshold velocities for aluminum). As with the Christiansen-Whipple BLE, the SRL BLE calculates the critical diameter d_c necessary to produce a component failure (via penetration or detached spall from the inner side of the component cover plate) based on the material characteristics and spacing of the structure panel and cover plate, as well as the characteristics of the impacting particle. The material characteristics are given as the MLI areal density $\rho_{AD,MLI}$, outer bumper thickness t_{ob}, and density ρ_{ob}, inner bumper thickness t_b, and internal component cover plate thickness t_w and yield strength $\sigma_{y,ksi}$. The spacing is given between the outer and inner bumpers s_1 as well as between the inner bumper and the component cover plate s_2. The impacting particle characteristics include the impact velocity v and angle θ, and the particle density ρ_p.

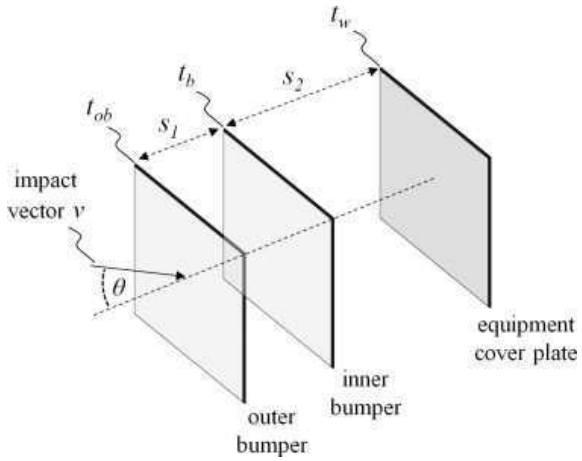

Figure 1. Typical SRL configuration [1].

Because the SRL BLE is designed to be applicable for a variety of internal component types, the results are moderately conservative and assume that the generation of spall or penetration definitively result in component failure. The typical SRL configuration is demonstrated in Fig. 1. Additionally, for the application of internal components behind varying structure panels from the described honeycomb panel or Whipple shield, the SRL provides special cases, specifically for stand-alone MLI (with or without stand-off to equipment) and single-wall shielding.

The SRL BLE was developed, calibrated and validated via a series of test campaigns both during and preceding the before noted ESA project [2][4][5][6].

For the purposes of the application of the SRL BLE in the PIRAT software, certain assumptions or simplifications were made. Because component damage must be assessed as statistically independent events, the application of cascading effects over multiple impacts or the influence of damage on one component to another are not considered. Due to the variety of possible equipment types, the cover plates for individual components are generalized to the two material characteristics listed previously (thickness and yield strength). For non-flat or angled surfaces with respect to the inner wall of the structure panel, the minimum distance between the cover plate and inner bumper is applied for s_2 [1].

2.2 Computation methodology

The analysis of component-level vulnerability is based on the output of the ESA MASTER debris flux model (MASTER-2009 and MASTER-2005). The discretized output of the stochastic model can be assessed directly in the vulnerability analysis, thereby avoiding the necessity of generating secondary probability distributions. For this reason, the PIRAT methodology is considered semi-deterministic.

The first step in completing the vulnerability analysis and enabling the computation of statistically independent component-level failure rates is the development of a satellite model and the definition of the mission and orbit parameters and the debris environment. The mission and orbit parameters and debris environment settings are applied to the selected debris model (MASTER-2009, MASTER-2005 or ORDEM2000).

Following the calculation of relevant debris fluxes using the selected debris flux model, the geometric analysis of the satellite physical architecture is performed. By discretizing potential threat directions based on a geodesic sphere, a database of impact angle based vulnerable projected areas for individual components and structure panels is created. "Visible" components are those which are exposed to the given threat direction (vulnerable projected area $A_v > 0$) either directly, or through a single structure panel.

Using the output of one of the debris flux models and the geometric analysis of the satellite physical architectures, the individual incoming fluxes are mapped to threat directions, whereby penetration and failure of visible structure panels and components are calculated using the SRL or similar BLE. Failure and penetration counts are aggregated based on flux ($1/m^2/yr$), projected vulnerable area (m^2) and mission duration (yr). Failure and penetration probabilities are determined based on failure rates using the equation derived from the discrete probability function in [1]:

$$P(\lambda > 0) = 1 - e^{-\lambda} \quad (1)$$

where λ = expected number of events. Fig. 2 demonstrates the methodology process flow.

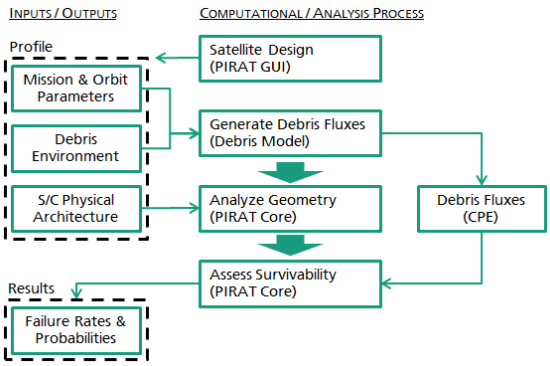

Figure 2. Interaction between PIRAT as a GUI, PIRAT as a computation core, the debris model and the I/O files.

In order to maintain statistical independence, during the survivability assessment phase, the debris fluxes generated by the debris flux models are evaluated individually. It is possible, within the definition of the satellite physical architecture and mission parameters, to define the mass of the satellite (kg) and a catastrophic threshold (J/g). Catastrophic impacts can be defined as fluxes leading to breakup (typically 40 J/g) [7] or simply total satellite failure. Fluxes exceeding the catastrophic threshold are labeled as such and are added to the overall catastrophic failure rate. The kinetic energies E_{kin} of the fluxes are calculated using the kinetic energy formula:

$$E_{kin} = 0.5 \cdot m_p \cdot v_p^2 \qquad (2)$$

with the projectile mass m_p and velocity v_p.

When implemented, catastrophic impacts are calculated based on the satellite structure projected area (discounting extruding panels and external components) and added to the total catastrophic flux rate for the satellite. Shadowing effects of external components are ignored in the catastrophic analysis.

Fluxes determined to be non-catastrophic are further assessed for structure panel penetration and external component failure. Penetrating fluxes are further assessed for internal component failure.

For each component, it is possible to specify whether the component should be analyzed for penetration, cratering (external components only), none or both. Non-analyzed components are ignored during the survivability assessment, except with regard to shadowing effects on other active components. Cratering failures are defined as individual impacts resulting in a proportion of damaged to total surface areas greater than a configurable threshold. Cratering is only assessed if no penetration failure has occurred, or if penetration has been disabled. As described previously, cascading conditions (such as multiple craters resulting in component failure) are precluded from the methodology.

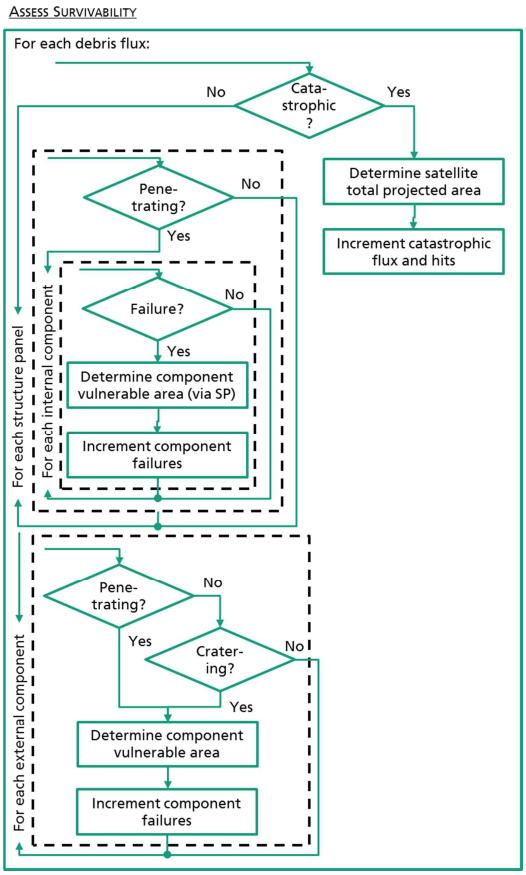

Figure 3. Flow diagram for debris processing (survivability assessment of individual components based on debris fluxes) in the computation core of PIRAT.

Table 1. Applied BLEs for configurable structure panel types, with regard to internal components.

	Structure Panel Penetration	Component Survivability
Double Bumper (Al)	Christiansen-Whipple [3]	SRL (*case S5/S6*) [2]
Double Bumper (CFRP)	Modified SRL [8]	Modified SRL [8]
Single Bumper (Al)	Cour-Palais [3]	SRL (*case S4*) [2]
Standalone MLI	N/A	SRL (*case S1/S2*) [2]
None	N/A	SRL (*case S3*) [2]

Fig. 3 demonstrates the survivability assessment flow and Tab. 1 and Tab. 2 list the applicable BLEs, based on structure panel type.

Table 2. Applied BLEs for external component failure analysis.

	Component Penetration	Surface Cratering
External Components	Cour-Palais [3]	Schäfer Cratering [9]

Following the completed aggregation of all failures for individual components, the resulting probabilities can be applied to the assessment of system or function vulnerability, using a Boolean logic model representing the satellite functional architecture [1].

3 MODELING THE SATELLITE

The demonstration satellite was defined as a geostationary earth observation satellite. In addition to the satellite structure, it is equipped with an avionics system, a communications system, a propulsion system, a power system and payloads.

3.1 Satellite structure

The structure is represented as a cube with a central tube (for main propulsion tanks) and internal shelves for mounting components. The outward-facing (Z+) and earth-facing (Z-) sides of the structure are composed of carbon-fiber reinforced plastic (CFRP) sandwich panels (SPs), with an opening in the Z+-direction for the main engine. The leading (X+) and trailing (X-) panels are solid double panel CFRP. The left and right facing structure sides (Y+ and Y-, respectively) are composed of a combination of aluminum double panel radiators (upper) and CFRP double structure panels (lower). On the left (from the direction of travel) side, an opening has been left in the CFRP for the exposure of star-trackers. In addition, several extrusions provide protection for certain external components like the batteries for the power system.

The modeling of the structure is accomplished by initially creating the satellite structure body, and meshing the side to a specific level that best approximates the borders of the individual panels. Following structure creation, individual structure panels can be modified based on their individual characteristics.

In this case, the meshing for the structure selected was 4 in the x- and y-directions and 6 in the z-direction. This allows for the approximation of the main engine exposure in the Z+-direction, the division between aluminum radiators and CFRP structure panels in the Y+ and Y- directions and the structure panel opening in the Y+ direction for the star-tracker exposure. Fig. 4 demonstrates the structure creation settings.

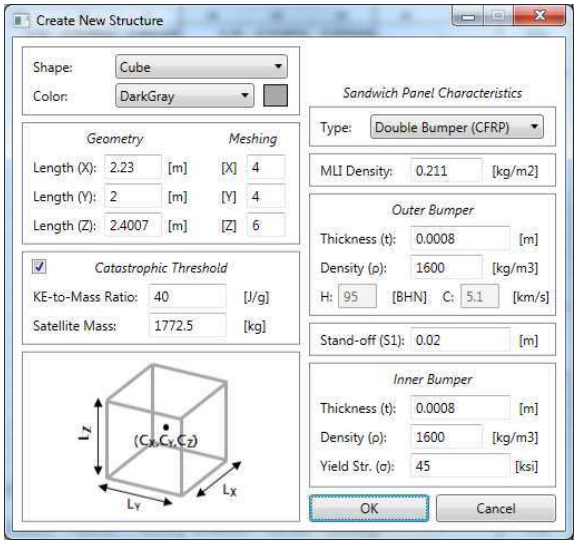

Figure 4. Satellite structure creation dialog with general SP characteristics.

The establishment of a catastrophic impact threshold is related to the satellite body itself (not applied to external components) and it is also configured in the satellite structure creation/modification dialog.

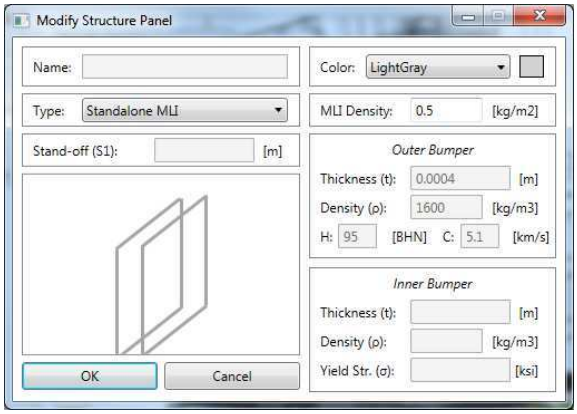

Figure 5. Example structure panel modification, for beta-cloth panels.

The individual structure panels, which deviate from the general SP characteristics defined in the structure creation, can be modified. The central four panels in the Z+-direction are modified to "Standalone MLI" type structure panels, with the beta-cloth characteristics considered in the increase MLI areal density. The missing two structure panels in the Y+ direction are modified to "None" and the aluminum panels are likewise modified. This is illustrated in the structure panel modification dialog in Fig. 5.

The internal and external shelves and extrusions are created as individual components. For shadowing analysis, a differentiation between internal and external components must be made. The central tube, for instance, is divided into internal and external subcomponents. Since the structural components are not analyzed for failure, their material characteristics are not relevant.

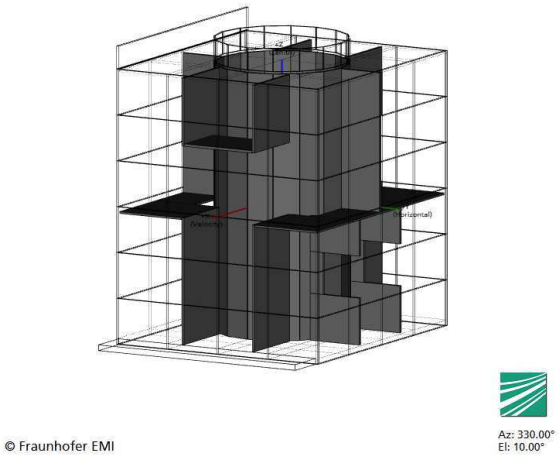

Figure 6. Internal view of the demonstration satellite structure from the left-leading direction.

Figure 7. External view of the demonstration satellite structure from the left-leading direction.

It should be considered that individual components are considered "bullet-proof" regardless of whether or not they are active. Components representing internal walls already constitute the third wall in the three-wall equation. BLEs have not been developed to consider a fourth or fifth wall.

Fig. 6 and Fig. 7 demonstrate the completed structure, as displayed in PIRAT.

3.2 Example components system: power system

The power system is selected as an example system because it contains both internal and external components, as well as components analyzed for penetration and for cratering failures.

The components of the power system consist of electronic boxes mounted on the inner walls of the structure panels (Y+-direction), solar array drive mechanisms (SADMs) mounted flush with the outer wall and extending inward, externally located batteries and solar panels. The e-boxes, SADMs and batteries are composed of aluminum, and the applicable material characteristics are applied. The e-boxes and batteries are modeled with cubes, while the SADMs are modeled as cylinders. The SADMs are modeled using two distinct cylinders. An internal 3D cylinder extends from the inner wall of the structure panel. An external cylinder with negligible depth is modeled on the external face. By aggregating the final failure counts of the two distinct components, a total failure rate of the component can be assessed. The use of multiple model components for the representation of single real components is necessary for modeling components spanning the structure panel or for components with a more complex form.

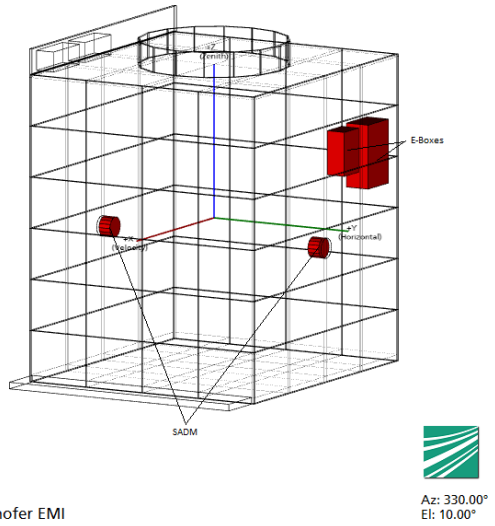

Figure 8. Internal components of the power system from the left-leading view.

The two external solar panels are modeled as cubes. Penetration of solar arrays does not necessarily constitute failure. In this case, cratering presents a greater threat to solar panels. For this reason, the solar panels are analyzed for cratering only. The cratering

threshold selected was 1.0 to represent total cratering of the solar array.

The batteries are located behind a structure panel in the right (in direction of flight) direction and exposed to the front, left and rear directions. Since the structure panel here is modeled as a "bullet-proof" external component, the results here can be considered liberal. Fig. 8 and Fig. 9 display the example power system.

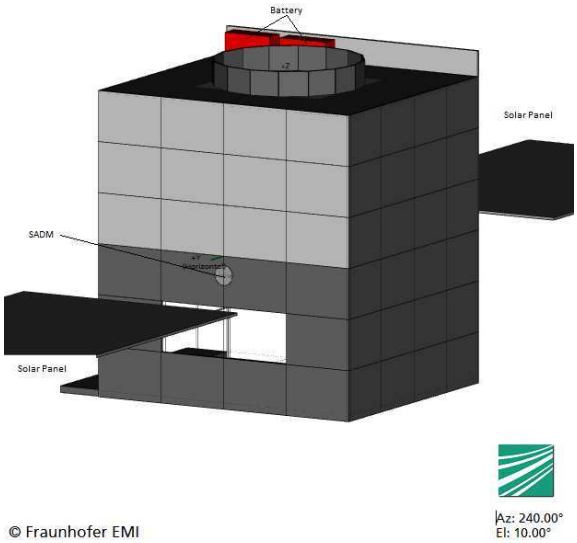

Figure 9. External components of the power system from the left-trailing view.

The same procedure is performed for the modeling of the other satellite sub-systems. Payloads can be created by constructing an additional structure from inactive components and mounting selected active components around the structure. The inactive components perform a shadowing effect on the components to be analyzed.

4 DEBRIS ENVIRONMENT

The orbit defined for the demonstration satellite was a geo-stationary orbit. The mission duration was specified for 7.5. The debris size interval ranges from 100 µm to 10 cm (lower trackable threshold), with a debris density of 2800 kg/m^3. All available debris and meteoroid populations available to master were applied.

Fig. 10 to Fig. 12 show the MM/SD flux distributions following the completion of the MASTER-2009 run. Fig. 10 demonstrates the significance of the meteoroid population in the geostationary orbit, with the majority of MM/SD in the 10 km/s to 20 km/s regime. From Fig. 11 and Fig. 12, it can be observed that the MM/SD population is fairly evenly distributed over the possible impact directions.

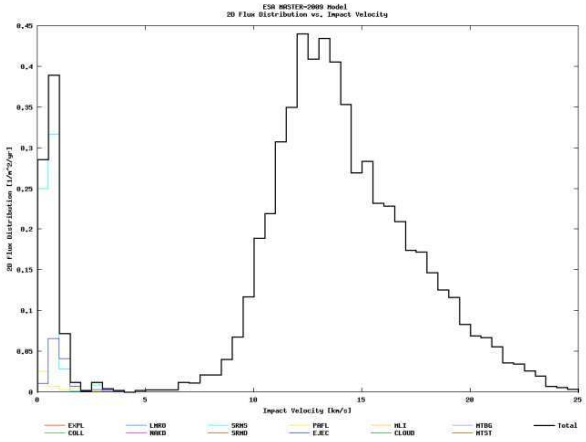

Figure 10. Debris flux (1/m^2/yr) distribution over velocity (km/s).

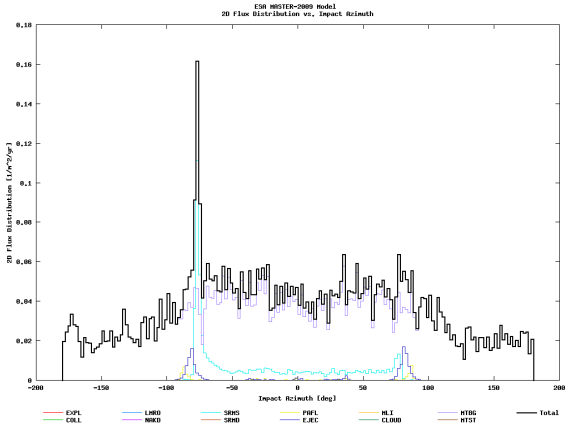

Figure 11. Debris flux (1/m^2/yr) distribution over azimuth (deg).

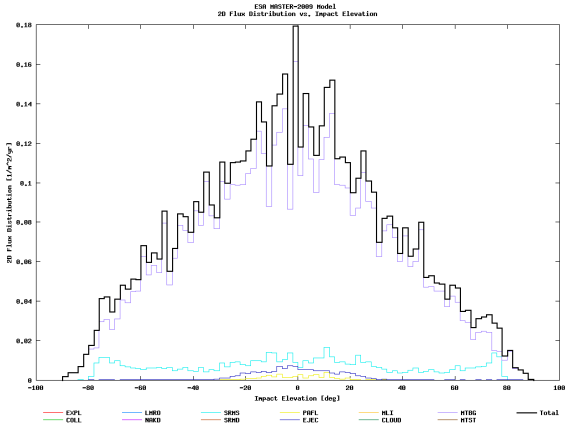

Figure 12. Debris flux (1/m^2/yr) distribution over elevation (deg).

5 RESULTS

By limiting the upper debris size to 10 cm, catastrophic impacts have been excluded. The non-catastrophic impact results can be visualized in several ways.

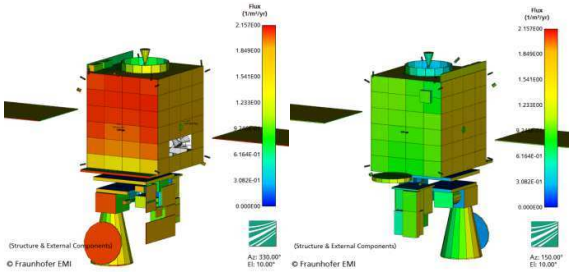

Figure 13. Incident flux (1/m^2/yr) from the left-leading (l.) and right-trailing (r.) perspectives on a linear scale.

The incident flux can be visualized on external components and structure panels on a face-by-face basis.

It can be observed in Fig. 13 and Fig. 14 that incident flux is significantly greater in (a) leading directions and (b) in locations with fewer shielding components.

In addition to impact flux, the results of the analysis can be viewed by total impacts per face, penetrations (SP only) and component failures. The color scale can be automatically generated or manually specified and the results are viewable on a logarithmic or linear scale. Fig. 15 and Fig. 16 demonstrate the comparison of penetration failures of internal and external components on a linear and logarithmic scale, respectively.

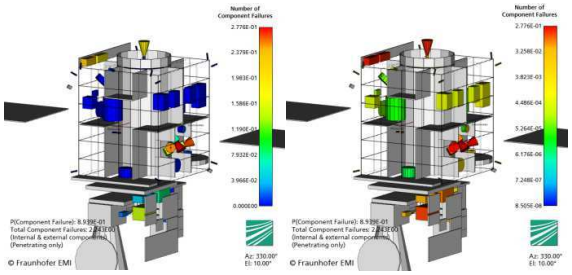

Figure 14. Penetration-only failures on linear (l.) and logarithmic (r.) scales.

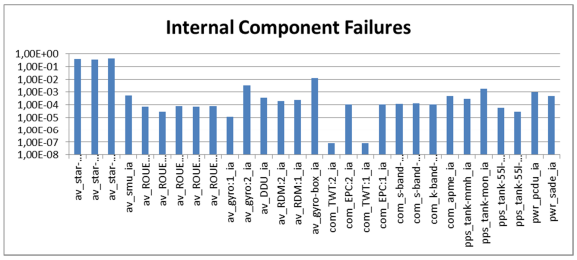

Figure 15. Internal component failures over mission time on a logarithmic scale.

Fig. 17 demonstrates the individual component failure rates. Because the exposed star-trackers showed drastically higher failure rates (due to exposure), the results are displayed on a logarithmic scale. The implementation of external component analysis can also be viewed, this time on a linear scale, in Fig. 18. The results are given both in expected failure counts and in failure probability over mission time.

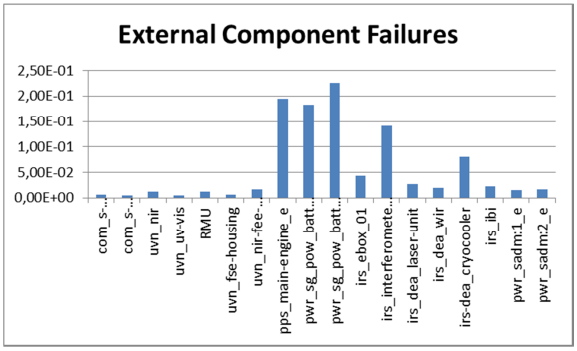

Figure 16. External component failures over mission time on a linear scale.

Following the initial analysis of the satellite, further iterative analyses can be performed by modifying material characteristics, thicknesses, component placement, etc. PIRAT only considers vulnerability due to MM/SD and must be therefore used in conjunction with other analyses, in which the effects of the changes on thermal or power budgets, etc. can be assessed. The final component-level results can be applied to tools such as SAVESPACE, which has also been developed in the framework of the P2-ROTECT project, or directly to existing failure tree analyses processes.

Within the P2-ROTECT project, this tool was used to analyze the satellites Sentinel-1 (LEO), Galileo (MEO) and Meteosat Third Generation (GEO). Fig 19. displays the visualization of the satellite designs in PIRAT.

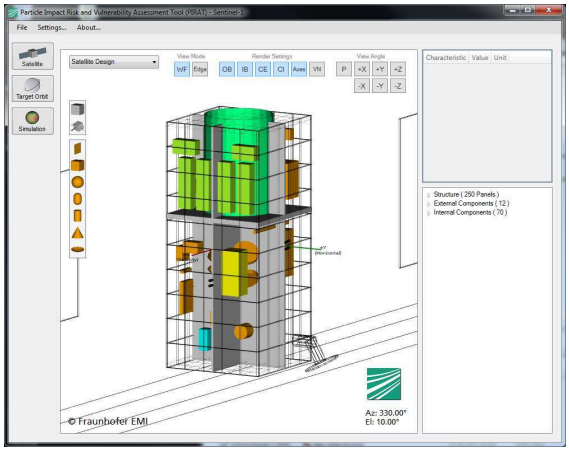

Figure 17. Screenshot of the Sentinel-1 satellite design in PIRAT.

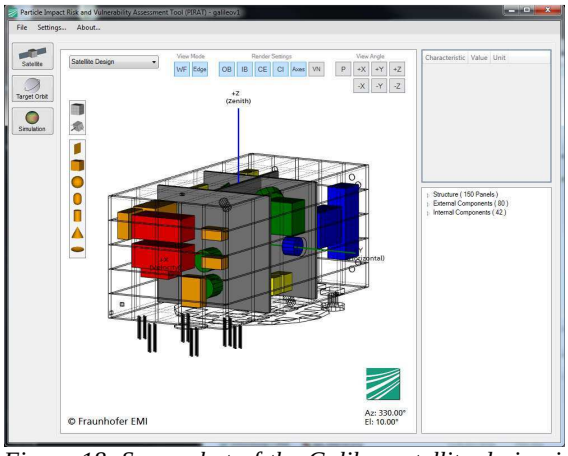

Figure 18. Screenshot of the Galileo satellite design in PIRAT.

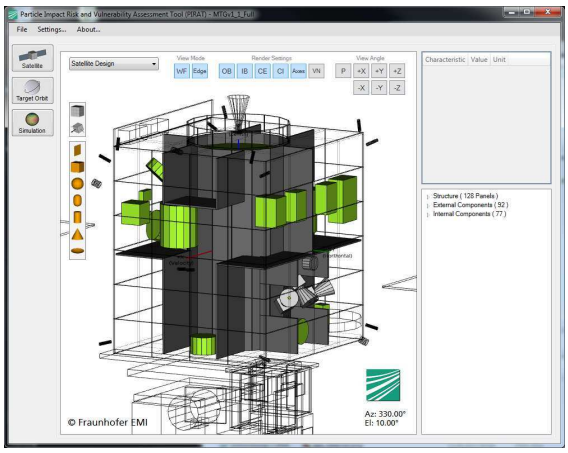

Figure 19. Screenshot of the MTG satellite design in PIRAT.

6 CONCLUSIONS

The PIRAT tool has been developed and applies the SRL BLE and the methodology developed in [1], which represent themselves a significant step with respect to vulnerability analyses of individual components in unmanned satellites due to MM/SD. In advantage to previous tools, PIRAT provides component level failure rates, based on penetration or cratering, of internal and external components.

A simple demonstration satellite has been modeled and analyzed using the tool, for which a selection of the process and results have been displayed and discussed. PIRAT provides a simple interface for the definition of satellite geometry, material characteristics and orbit and debris environment specifications. By applying the results derived from a PIRAT analysis during the initial design phases of a satellite, the user can quickly generate feedback in terms of failure rates and probability, thus enabling early modifications to lower satellite vulnerability.

7 ACKNOWLEDGEMENTS

This work was funded by the European Commision via the Framework Programme 7 under contract number 262820, in the project P2-ROTECT.

8 REFERENCES

1. Welty, N., Rudolph, M., Schäfer, F., Apeldoorn, J. and Janovsky, R. (2013). Computational methodology to predict satellite system-level effects from impacts of untrackable space debris, *Acta Astronautica* **88**, 35–43

2. Schäfer, F., Ryan, S., Lambert, M., Putzar, R. (2008). Ballistic limit equation for equipment placed behind satellite structure walls. *Int. J. Impact Eng.* **35**, 1784–1791

3. Christiansen, E. (1993). Design and performance equations for advanced meteoroid and debris shields. *Int. J. Impact Eng.* **14**, 145–156

4. Schäfer, F., Putzar, R., Lambert, M. (2008). Vulnerability of satellite equipment to hypervelocity impacts, *Proc. 49th International Astronautical Congress, Sept. 29–Oct. 3, 2008*, Glasgow, Scotland

5. Putzar, R., Schäfer, F., Lambert, M. (2008). Vulnerability of spacecraft harnesses to hypervelocity impacts. *Int. J. Impact Eng.* **35**, 1738–1734

6. Putzar, R., Schäfer, F., Stokes, H., Chant, R., Lambert, M. (2005). Vulnerability of spacecraft electronic boxes to hypervelocity impacts. *Proc. 56th International Astronautical Congress, Oct. 17–21, 2005*, Fukuoka, Japan

7. McKnight, D., Maher, R., Nagl, L. (1995). Refined algorithms for structural breakup due to hypervelocity impact. *Int. J. Impact Eng.* **17**, 547–558

8. Ryan, S., Schäfer, F., Destefanis, R., Lambert, M. (2008). A ballistic limit equation for hypervelocity impacts on composite honeycomb sandwich panel satellite structures. *Advances in Space Research* **41**, 1152–1166

9. Schäfer, F., Geyer, T., Schneider, E., Rott, M., Igenbergs, E. (2001). Degradation and destructions of optical surfaces by hypervelocity impact. *Int. J. Impact Eng.* **26**, 683–698